Calculation of back-reflected intensities of a Na-atom beam by a standing evanescent E-M field

1993 J. Phys.: Condens. Matter 5 4665

(http://iopscience.iop.org/0953-8984/5/27/011)

J. Phys.: Condens. Matter 5 (1993) 4665–4676. Printed in the UK

Calculation of back-reflected intensities of a Na-atom beam by a standing evanescent E–M field

J Murphy†, P Goodman† and Andrew Smith‡

† School of Physics, University of Melbourne, Parkville, Victoria 3052, Australia
‡ Department of Physics, Monash University, Clayton, Victoria 3168, Australia

Received 19 November 1992, in final form 13 April 1993

Abstract. A method is described for the computation of the back-scattered intensities of atomic beams, diffracted from the evanescent field generated outside an optical plate by internal counter-propagating laser beams. The method derives from a procedure developed for the similar but importantly differing problem of low-energy electron diffraction (LEED). Modifications to that theory required for the present problem bring the equations closer to the reflection high-energy electron diffraction (RHEED) solution proposed by Ichimiya. Preliminary calculations for the strong-field case indicate that diffracted beams occur with intensities of 7% and 8% of the incident beam which if correct should lead to detectable diffraction effects.

1. Introduction

Recently, atomic de Broglie wave diffraction by a standing evanescent wave field has been investigated both theoretically [1] and experimentally [2], for the case of a monochromatized Na-atom beam incident on the vacuum interface of a light-transmitting quartz block. The solution suggested in [1], namely that of a Green's function iteration, has been tried previously in electron diffraction and found to be very slowly convergent. This problem, present in the high-energy case of forward scattering, is likely to be exacerbated in the case of the complete solution which includes both backwards and forwards scattering. The alternative approach, known in electron diffraction physics, as 'multi-slice' [3], has all the advantages of a closed, summed solution which is limited to elastic or pseudo-elastic processes. This formulation has been expanded to a complete solution which includes back-scattering by Lynch and Moodie [4] and Lynch and Smith [5]. For the present problem, involving the transitions of a two-level atom, this description is valid and the method should transfer, with consequent substantial savings in computation effort and time when compared with the above method [1].

The present paper gives firstly a brief discussion of the approach and a few basic equations, and secondly some initial results, for both weak- and strong-field cases.

2. Solutions to Schrödinger's equation

The time-independent Schrödinger equation may be written as

$$\nabla_r^2\psi_r + \gamma(E - V)\psi_r = 0 \qquad \text{with } \gamma = 2m/\hbar^2 \tag{1}$$

0953-8984/93/274665+12$07.50

in a completely general way, where r represents spatial coordinates in one, two or three dimensions according to the particular problem. In applications in three-dimensional space involving a potential V periodic only two dimensions it is usual to choose the coordinates x, y, z so the unique direction definable in most laboratory experiments coincides with either the y (or z) direction, and to Fourier transform the equation with respect to the non-unique directions in which V is periodic (xz/xy) ('semi-reciprocal' space: [1,4]). This then permits us to write (1) in matrix form and as a second-order differential equation in one dimension as

$$d^2\psi/d^2y = -\mathbf{M}(y)\psi \tag{2}$$

with y as the unique direction, and where $\mathbf{M} = \gamma(\mathbf{E} - \mathbf{V})$ is a square matrix in which $\mathbf{E}$ and $\mathbf{V}$ form the diagonal and off-diagonal terms respectively, i.e. the diagonal elements contain the terms $k^2(y)$ (with $k = 2\pi/\lambda$), and the off-diagonal elements contain the Fourier coefficients of the optical potential.

There is some advantage at this stage in considering the solution to the transmission electron diffraction case, where for example Cowley [6] has shown that the matrix $\mathbf{M}$ may be replaced to a good approximation by a matrix $\mathbf{L}$ in which the diagonal terms have been linearized (the so-called 'forward-scattering' approximation). Using the coordinates of our present problem, where the free (non-quantized) momentum is restricted to the y direction and there is no z dependence in the equation, the forward-scattering solution for Schrödinger's equation is

$$\psi(h, y) = \exp(i\mathbf{L}y)\psi(0) = \mathbf{S}\psi(0) \tag{3}$$

where h is the diffraction space coordinate reciprocal to x and ψ is now used to denote the wavefunction in 'semi-reciprocal' space coordinates. This solution applies provided a matrix $\mathbf{L}$ can be found for which the interaction potential (off-diagonal) terms are independent of y. The diagonal terms consist of the y-resolved momenta k_y which are not functionally dependent on y. This condition will be referred to throughout this paper, or is an implied condition of future equations. The operator form of solution to (3) using the scattering matrix $\mathbf{S} = \exp(i\mathbf{L}y)$, may be brought to numerical evaluation, either through the Taylor (i.e. Born series) expansion

$$\mathbf{S} = 1 + (i\mathbf{L}y) + (i\mathbf{L}y)^2/2! + (i\mathbf{L}y)^3/3! + \ldots \tag{4}$$

or through the product expansion

$$\mathbf{S} = \exp(i\mathbf{L}\,\delta y_1)\exp(i\mathbf{L}\,\delta y_2)\exp(\mathbf{L}\,\delta y_3)\ldots \tag{5}$$

with $y = \sum_i \delta y_i$. Equations (4) and (5) formally represent alternative approaches to solving (1), namely the Born series expansion, and the multi-slice expression (analogous to the Feynman path integral approach [3]), respectively.

In the more general case including back-scattering the complete second-order equation (2) must be solved. Adopting now a method for reducing the order of the differential equation, given in [4], we substitute the first differential of the wavefunction

$$\psi' = d\psi/dy$$

giving

$$d\psi'/dy = -\mathbf{M}(y)\psi.$$

Introducing 'supermatrix' notation [7,4] allows us more compact notation. Hence,

$$d\Psi/dy = \mathcal{M}(y)\Psi \tag{6}$$

becomes our master equation, with Ψ a supercolumn vector of order two whose elements are the infinite column vectors ψ, ψ', that is

$$\Psi = \begin{pmatrix} \psi \\ \psi' \end{pmatrix}$$

i.e. the scattering amplitudes and their derivatives for the various diffracted directions, and

$$\mathcal{M}(y) = \begin{pmatrix} \mathbf{0} & \mathbf{I} \\ -\mathbf{M}(y) & \mathbf{0} \end{pmatrix}$$

is the 2×2 matrix whose elements are square matrices: $\mathbf{M}(y)$ has the elements defined previously; $\mathbf{I}$ is the identity matrix of the same order as $\mathbf{M}$, and $\mathbf{0}$ is the equivalent null matrix.

If $\mathcal{M}$ is independent of y, the solution to (6) may be written as

$$\Psi = \exp(\mathcal{M}y)\Psi(0) = \mathcal{S}\Psi(0). \tag{7}$$

This equation is now analogous to (3), but in supermatrix form so that both backward and forward scattering are included. The solution differs from the analytical form of (7) when $\mathcal{M}$ is dependent of y; it is then useful to consider slicing the operator in order to obtain matrices which may be considered as independent of y, following the logic of (5).

Hence, expanding $\mathcal{S}$ as the product series

$$\mathcal{S} = s_p s_{p-1} \ldots s_1 \tag{8}$$

gives us the multi-slice expansion, in which the general term $s_{p-n} = \exp(\mathcal{M}_{p-n}\,\Delta y_{p-n})$ is called the 'slice operator'. These expressions will be made applicable by taking slices normal to y sufficiently thin so that the potential is effectively constant within each slice. In (7) the complex exponential of (3) is not evident, although required for elastic scattering. The apparent inconsistency is resolved in the derivation of $\exp(\mathcal{M}\Delta)$: taking a constant slice thickness $\delta y = \Delta$, we may expand

$$\exp(\mathcal{M}\Delta) = \exp\left[\begin{pmatrix} \mathbf{0} & \mathbf{I} \\ -\mathbf{M} & \mathbf{0} \end{pmatrix}\Delta\right] = \mathbf{I} + \begin{pmatrix} \mathbf{0} & \mathbf{I} \\ -\mathbf{M} & \mathbf{0} \end{pmatrix}\Delta + \begin{pmatrix} -\mathbf{M} & \mathbf{0} \\ \mathbf{0} & -\mathbf{M} \end{pmatrix}\frac{\Delta^2}{2!} - \begin{pmatrix} \mathbf{0} & -\mathbf{M} \\ \mathbf{M}^2 & \mathbf{0} \end{pmatrix}\frac{\Delta^3}{3!} \cdots$$

On the other hand the terms may be combined differently to give

$$\exp(\mathcal{M}\Delta) = \Big| - \Big|\frac{(\mathbf{M}^{1/2}\Delta)^2}{2!}\mathbf{I} + \frac{(\mathbf{M}^{1/2}\Delta)^4}{4!}\mathbf{I} - \ldots + (\mathbf{M}^{1/2}\Delta)\begin{pmatrix} \mathbf{0} & \mathbf{M}^{-1/2} \\ -\mathbf{M}^{-1/2} & \mathbf{0} \end{pmatrix} - \left(\frac{\mathbf{M}^{1/2}\Delta}{3!}\right)^3\begin{pmatrix} \mathbf{0} & \mathbf{M}^{-1/2} \\ -\mathbf{M}^{-1/2} & \mathbf{0} \end{pmatrix} + \left(\frac{\mathbf{M}^{1/2}\Delta}{5!}\right)^5\begin{pmatrix} \mathbf{0} & \mathbf{M}^{-1/2} \\ -\mathbf{M}^{-1/2} & \mathbf{0} \end{pmatrix} - \cdots$$

This may be written in matrix form as

$$\exp(\mathcal{M}\Delta) = \frac{1}{2}\begin{pmatrix} \exp(\mathrm{i}\,\Delta\mathbf{M}^{1/2}) + \exp(-\mathrm{i}\,\Delta\mathbf{M}^{1/2}) & -\mathrm{i}\mathbf{M}^{-1/2}(\exp(\mathrm{i}\,\Delta\mathbf{M}^{1/2}) - \exp(-\mathrm{i}\,\Delta\mathbf{M}^{1/2})) \\ \mathrm{i}\,\mathbf{M}^{1/2}(\exp(\mathrm{i}\,\Delta\mathbf{M}^{1/2}) - \exp(-\mathrm{i}\,\Delta\mathbf{M}^{1/2})) & \exp(\mathrm{i}\,\Delta\mathbf{M}^{1/2}) + \exp(-\mathrm{i}\,\Delta\mathbf{M}^{1/2}) \end{pmatrix} \tag{9a}$$

which in turn condenses into

$$\exp(\mathcal{M}\Delta) = \begin{pmatrix} \cos(\mathbf{M}^{1/2}\Delta) & \mathbf{M}^{-1/2}\sin(\mathbf{M}^{1/2}\Delta) \\ -\mathbf{M}^{1/2}\sin(\mathbf{M}^{1/2}\Delta) & \cos(\mathbf{M}^{1/2}\Delta) \end{pmatrix}. \tag{9b}$$

It is clear now that (9*a*) above is the complex exponential equivalent to that in (3), with the inclusion of the backward scattering, giving the analytical advantage of yielding the dual forms of Born series expansion and unitary matrix, following the path shown earlier in (4) and (5) for forward scattering.

The operator (9*b*) is evaluated numerically using a Jacobi routine which diagonalizes this scattering matrix by a complex plane rotation

$$\chi^{\dagger}\mathbf{M}\chi = \mu$$

where χ and $\chi^{\dagger}$ represent a unitary matrix and its inverse, and μ is the diagonal matrix with the eigenvalues $\mu_1, \mu_2, \ldots, \mu_n$, as entries. The slice operator may now be written as

$$\exp(\mathcal{M}_p\Delta)_p = \chi\begin{pmatrix} \cos(\mu_p^{1/2}\Delta) & \mu_p^{-1/2}\sin(\mu_p^{1/2}\Delta) \\ -\mu_p^{1/2}\sin(\mu_p^{1/2}\Delta) & \cos(\mu_p^{1/2}\Delta) \end{pmatrix}\chi^{\dagger} \tag{10}$$

for the pth slice.

In general the equal-thickness slices will not have the same potential, so the μs will be slice dependent. It is a particular feature of this expansion that (8) can be evaluated by the sequential multiplications of the slice operator (10), with application of boundary conditions needed to determine the amplitudes of the diffracted beams being carried out as a final step.

3. The Hajnal–Opat equations

Figure 1 shows the geometry of the experiment for reflection–diffraction of atoms from a standing evanescent wave field. We define ω_0 and ω as the characteristic frequency of the two-level atom and the frequency of the incoming light beam respectively. This beam directed from a laser into the quartz block is retro-reflected to give a standing wave at the quartz–vacuum interface. Under conditions of total internal reflection, a standing evanescent wave field is generated above the interface and extending into the vacuum. Upon entering this vacuum field, the ground state atom experiences a gradient force which is repulsive or attractive for a positive or negative detuning $\Delta\omega = \omega - \omega_0$, in agreement with the Kramers–Kronig relationship.

The Hajnal–Opat formulation [1] of Schrödinger's equation for this interaction is given as

$$(\mathrm{d}^2/\mathrm{d}y^2 + K_{yn}^2)\psi_n(y) = -(2\epsilon E_0 m_{\mathrm{A}}/\hbar^2)[\psi_{n+1}(y) + \psi_{n-1}(y)]\exp(-qy) \tag{11}$$

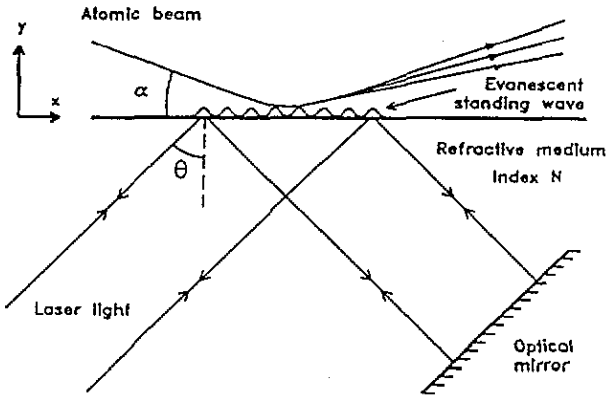

Figure 1. Sketch of the experimental set-up used by Opat and Hajnal for reflection–diffraction of waves from a standing evanescent wave field.

with m_A the atomic mass, and where

$$K_{yn}^2 \equiv K_y^2 - Q^2n^2 - 2nQK_x - (2m_A/\hbar)(\omega_0 - \omega) \qquad n \text{ odd} \tag{12}$$

$$K_{yn}^2 \equiv K_y^2 - Q^2n^2 - 2nQK_x \qquad n \text{ even.} \tag{13}$$

$K_{xn} \equiv K_x + nQ$, where $\hbar Q$ = transferred photon momentum, along the x direction, while Q and q are the x- and y-resolved components of the electromagnetic wave vector given by

$$Q\boldsymbol{h} + \mathrm{i}q\boldsymbol{l} = (\omega/c)N(\sin\theta)\boldsymbol{h} + \mathrm{i}(\omega/c)(N\sin^2\theta - 1)^{1/2}\boldsymbol{l}$$

where N is the refractive index of the quartz block, and $\boldsymbol{h}$ and $\boldsymbol{l}$ are the unit vectors of momentum parallel to the x and y directions [1], and

$$\epsilon E_0 = \langle a|\mathcal{E}|b\rangle E_0$$

where $\mathcal{E}$ is the electric dipole operator and E_0 is the electric field amplitude.

An incoming atom, which we assume to be a plane wave, is scattered by the electric field and emerges in plane-wave solutions that must satisfy (11). Initially the atom is in the ground state. In making a transition to the excited state by the absorption of a photon from either of the counter-propagating evanescent waves there will correspondingly be a positive or negative increment in the x momentum of the atom leading to a transition to either of the $n = \pm 1$ (odd) diffraction orders. A further transition back to the ground state by stimulated emission will then result in a further momentum exchange due to the emission of a photon to either counter-propagating wave, resulting in a transition from $n = 1$ to $n = 1 \pm 1 \rightarrow 2, 0$, representing a return to even states. Hence, the ground and excited state atoms are to be found in the n-even and n-odd momentum states respectively. Furthermore, for n-odd K_{yn} has a contribution proportional to the detuning $(\omega - \omega_0)$ given by the last term in (12) which cancels for n even. Hence the odd diffraction orders will move in position across the stationary even orders as the detuning is varied.

Hajnal and Opat used the integral equation method to solve (11), using the solution

$$\Psi_n(Y) = \delta_{n0}\exp(-\mathrm{i}K_0Y) - \int G_n(Y - Y_0)P(Y_0)\,\mathrm{d}Y$$

where

$$P(Y) = \gamma \mu E_0[(\Psi_{n+1}(Y_0) + \Psi_{n-1}(Y_0)] \exp(-qY_0))$$

and G_n is a Green function:

$$G_n(Y - Y_0) = \exp(\mathrm{i}\, K_{yn}|Y - Y_0|)/2\mathrm{i}\, K_{yn}.$$

This is an iterative method, where Ψ_n is cast in an integral series form which identifies with the Born series (see (4)). This series is slowly convergent when E_0 is large.

4. Computed intensities using the Lynch–Smith procedure

The alternative method using LEED theory involves rewriting (11) in matrix notation as

$$\frac{\mathrm{d}^2}{\mathrm{d}Y^2}\begin{pmatrix}\psi_{-n}\\ \vdots \\ \psi_n\end{pmatrix} = -\mathbf{M}(y)\begin{pmatrix}\psi_{-n}\\ \vdots \\ \psi_n\end{pmatrix} \tag{14}$$

where

$$\mathbf{M}(y) = \begin{bmatrix} \vdots & \vdots & \mathbf{0} & \mathbf{0} & \mathbf{0} \\ \vdots & K_{y-1}^2 & \alpha & \mathbf{0} & \mathbf{0} \\ \mathbf{0} & \alpha & K_{y0}^2 & \alpha & \vdots \\ \mathbf{0} & \mathbf{0} & \alpha & K_{y+1}^2 & \vdots \\ \mathbf{0} & \mathbf{0} & \vdots & \vdots & \vdots \end{bmatrix} \qquad \alpha = \frac{2m_{\mathrm{A}}\epsilon E_0}{\hbar^2}\exp(-qy)$$

and slicing the potential normal to the y-axis so that slice boundaries are parallel to the optical interface in the experiment. If we wish to keep slice thicknesses Δy constant, we need to choose a slice sufficiently thin that in the region of maximum field gradient neighbouring $y = 0$, the interaction term may be assumed constant; i.e. we wish to map the $\exp(-qy)$ field dependence as a step function in y, as shown in figure 2. This allows us to adopt the 'zero-layer' approximation of electron diffraction [4], with y-independent interaction terms in each slice.

Lynch–Smith procedures then involve applying boundary conditions to the cumulative product of (8). Writing

$$\Psi(y) = \mathbf{S}\Psi_0 = \begin{pmatrix} S_{11} & S_{12} \\ S_{21} & S_{22}\end{pmatrix}\begin{pmatrix}\psi_0 \\ \psi_0'\end{pmatrix} \tag{15}$$

$$\psi_{\mathrm{I}}(y) = \exp(\mathrm{i}\,\mathbf{K}_{\mathrm{I}}y)\boldsymbol{A} + \exp(-\mathrm{i}\,\mathbf{K}_{\mathrm{I}}y)\boldsymbol{B}$$

for region I, as defined in figure 2, where $\mathbf{K}_{\mathrm{I}}$ denotes a diagonal matrix with K_y terms as elements, and

$$\boldsymbol{A} = \begin{pmatrix}1\\0\\0\\\vdots\end{pmatrix} \qquad \boldsymbol{B} = \begin{pmatrix}b_1\\b_2\\b_3\\\vdots\end{pmatrix}.$$

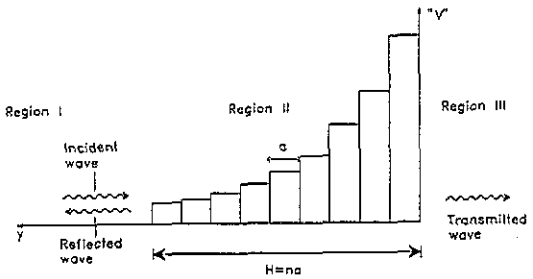

Figure 2. Diagram showing the computational scheme for slicing the optical potential in region II. Here, region I contains the source and detector system and region III represents the refractive medium. Steps show a qualitative similarity with the $\exp(-qy)$ field dependence.

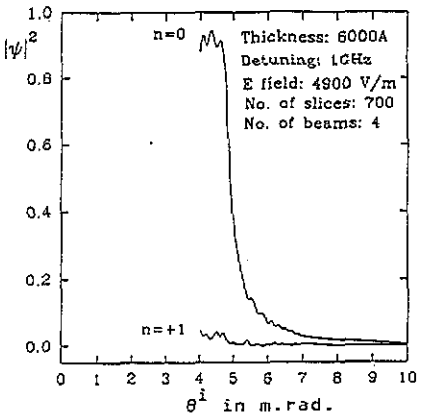

Figure 3. Intensities of specular ($n = 0$) and $n = +1$ diffracted beam obtained from a 4-beam calculation for the weak-field case ($E = 4900$ V m^{-1}) and field depth of 6000 Å, using 700 slices and a detuning of 1 GHz.

For region III, since there is no wave incident from the right

$$\Psi_{\mathrm{III}} = \exp(\mathrm{i}\,\mathbf{K}_{\mathrm{I}} y)E \qquad \mathbf{K}_{\mathrm{I}} = \mathbf{K}_{\mathrm{III}}.$$

Applying boundary conditions

$$\begin{aligned} \exp(\mathrm{i}\,\mathbf{K}_{\mathrm{I}} H)E &= S_{11}(A+B) + S_{12}\mathbf{K}_{\mathrm{I}}(A-B) \\ \mathrm{i}\,\mathbf{K}_{\mathrm{I}}\exp(\mathrm{i}\,\mathbf{K}_{\mathrm{I}} H)E &= S_{21}(A+B) + S_{22}\mathrm{i}\,\mathbf{K}_{\mathrm{I}}(A-B) \end{aligned} \tag{16}$$

with $H = na$ the total depth of the potential (n is the number of slices and a is their width). We may determine B in terms of A as

$$B = (\alpha+\beta)^{-1}(\alpha-\beta)A$$

where $\alpha = S_{22}\mathrm{i}\,\mathbf{K}_{\mathrm{I}} + \mathbf{K}_{\mathrm{I}} S_{12}\mathbf{K}_{\mathrm{I}}$ and $\beta = -S_{21} + \mathrm{i}\,\mathbf{K}_{\mathrm{I}} S_{11}$.

By applying boundary conditions only at the interfaces of regions II and I and of II and III the calculation proceeds rapidly. However, because we have a repulsive potential, there are a significant number of classically forbidden or tunnelling states corresponding to negative values of K_{yn}^2 on the diagonal of $\mathbf{M}$, which are a potential source of numerical instability in a calculation.

We consider first the 'weak-field case' (with $E_0 = 4.900$ V m^{-1} and a decay length of 2600 Å), as it is reasonable here to exclude terms with $K_{yn}^2 < 0$ at the angles of incidence considered. Subsequent diagonalization will not then produce negative eigenvalues.

Results are plotted in figure 3 as a function of incident angle for a 700-slice calculation and for a field depth of 6000 Å. The results are stable for $\theta_i > 4$ mrad and are essentially similar to those obtained in [1]. For $\theta_i < 4$ mrad, since $K_y^{\mathrm{inc}} = K_0 \sin\theta_i$, the incident kinetic energy falls below the effective barrier potential, promoting tunnelling states with $K_{yn}^2 < 0$.

In table 1 the rate of convergence obtained for decreasing slice thickness is seen by comparing the results for 100, 500 and 700 slices, for the fixed field depth of 6000 Å. It can be seen from figure 3 that the strongest diffracted beam ($n = +1$) is still very weak compared to the specular beam; the $n = -1$ beam is still weaker and off the scale of the plot. This justifies the restriction to four beams, a requirement of the condition for excluding negative values of K_{yn}^2.

Table 1. Results obtained by slicing the optical potential into 100, 500 and 700 slices respectively in the weak-field case, shown here for the +1 and zero-order diffracted beams.

	100 slices		500 slices		700 slices	
θ_{inc} (mrad)	$n=+1$	$n=0$	$n=+1$	$n=0$	$n=+1$	$n=0$
4	0.254×10^{-1}	0.931E+00	0.604×10^{-1}	0.880	0.482×10^{-1}	0.884
5	0.210×10^{-1}	0.337E+00	0.976×10^{-2}	0.364	0.973×10^{-2}	0.367
6	0.118×10^{-2}	0.712×10^{-1}	0.733×10^{-2}	0.674×10^{-1}	0.724×10^{-2}	0.680×10^{-1}
7	0.454×10^{-2}	0.366×10^{-1}	0.644×10^{-2}	0.276×10^{-1}	0.621×10^{-2}	0.278×10^{-1}
8	0.200×10^{-2}	0.140×10^{-1}	0.439×10^{-3}	0.173×10^{-1}	0.395×10^{-3}	0.175×10^{-1}
9	0.153×10^{-2}	0.923×10^{-2}	0.135×10^{-3}	0.103×10^{-1}	0.901×10^{-4}	0.103×10^{-1}
10	0.976×10^{-4}	0.666×10^{-2}	0.611×10^{-3}	0.524×10^{-2}	0.706×10^{-3}	0.521×10^{-2}

5. Reformulation of boundary conditions for the strong-field case

When $\mu_p^{1/2}$ in (10) is imaginary the trigonometric functions in the slice operator become hyperbolic. This is the cause of the instability in the calculation. The hyperbolic terms are entirely physical as the slice operator still conserves flux (or 'probability'). In practice these terms quickly become many orders of magnitude greater than the trigonometric terms, rendering the calculation unstable, considering the limitations of the computer. The use of thinner slices allows the terms within each slice to be manageable in themselves; however, this also necessitates the use of *more* slices and the total operator contains the same unmanageable terms as before. If, however, boundary conditions are applied after each slice, stability can be maintained incrementally, and computer overload avoided. For this procedure we envisage a vacuum separation between neighbouring slices Δy, which may have an arbitrarily small value, as indicated diagrammatically in figure 4. It can easily be shown that the solution becomes physically correct in the limit $\Delta y \to 0$.

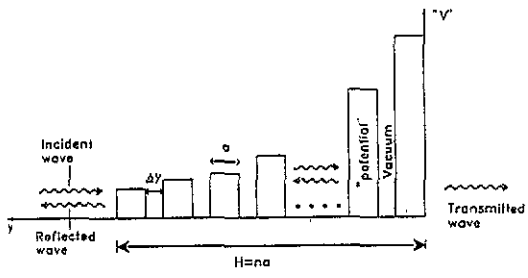

Figure 4. Modification of figure 2 where the slices of thickness a are shown separated by a vacuum space Δy.

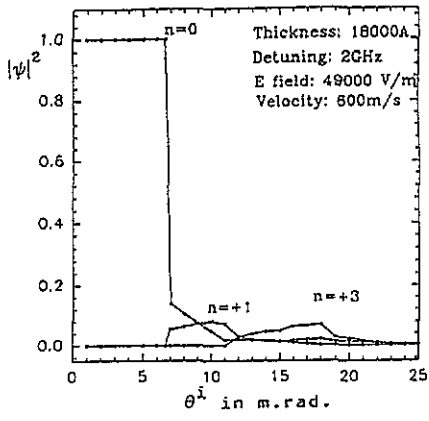

Figure 5. Intensities of specular ($n = 0$) and +1, +3 diffracted beams for the strong-field case ($E = 49000$ V m^{-1}) and a field depth of 18000 Å. From a 13-beam calculation using 1 Å slices and 2 GHz detuning.

The calculation begins at the slice adjacent to the quartz interface, since there is no reflected wave incident on the exit face for this slice, with the crystal being treated as a

sink for the de Broglie waves. Letting

$$U_p = \exp(\mathrm{i}\,\mathbf{K}_\mathrm{I} pa) \qquad U_p^* = \exp(-\mathrm{i}\,\mathbf{K}_\mathrm{I} pa)$$

the boundary conditions for this pth slice (the starting slice for our calculation) adjacent to the quartz interface are given by

$$\begin{aligned} U_{p+1}\mathbf{A}_{p+1} &= S_{11}^p(U_p\mathbf{A}_p + U_p^*\mathbf{B}_p) + S_{12}^p \mathrm{i}\,\mathbf{K}_\mathrm{I}(U_p\mathbf{A}_p - U_p^*\mathbf{B}_p) \\ \mathrm{i}\,\mathbf{K}_\mathrm{I} U_{p+1}\mathbf{A}_{p+1} &= S_{21}^p(U_p\mathbf{A}_p + U_p^*\mathbf{B}_p) + S_{22}^p \mathrm{i}\,\mathbf{K}_\mathrm{I}(U_p\mathbf{A}_p - U_p^*\mathbf{B}_p). \end{aligned} \tag{17}$$

The U^*-terms in (17) still contain elements proportional to $\exp(\mathbf{K}_\mathrm{I} y)$ when the elements of $\mathbf{K}_\mathrm{I}$ are imaginary. However, by first taking the products

$$U_p\mathbf{A}_p = \Phi_p^+ \qquad U_p^*\mathbf{B}_p = \Phi_p^-$$

equation (17) becomes

$$\begin{aligned} \Phi_{p+1}^+ &= S_{11}^p(\Phi_p^+ + \Phi_p^-) + S_{12}^p \mathrm{i}\,\mathbf{K}_\mathrm{I}(\Phi_p^+ - \Phi_p^-) \\ \mathrm{i}\,\mathbf{K}_\mathrm{I}\Phi_{p+1}^+ &= S_{21}^p(\Phi_p^+ + \Phi_p^-) + S_{22}^p \mathrm{i}\,\mathbf{K}_\mathrm{I}(\Phi_p^+ - \Phi_p^-) \end{aligned} \tag{18}$$

and no longer contains unmanageable terms. The equations in (18) are of exactly the same form as equations (16), and therefore by inspection

$$\Phi_p^- = (\alpha_p + \beta_p)^{-1}(\alpha_p - \beta_p)\Phi_p^+ = \gamma_p \Phi_p^+.$$

The equations relating the pth slice to the $(p-1)$th slice, which has both transmitted and reflected waves at both surfaces, now appears as

$$\begin{aligned} \Phi_p^+ + \Phi_p^- &= S_{11}^{p-1}(\Phi_{p-1}^+ + \Phi_{p-1}^-) + S_{12}^{p-1}\mathrm{i}\,\mathbf{K}_\mathrm{I}(\Phi_{p-1}^+ - \Phi_{p-1}^-) \\ \mathrm{i}\,\mathbf{K}_\mathrm{I}\Phi_{p+1}^+ &= S_{21}^{p-1}(\Phi_{p-1}^+ + \Phi_{p-1}^-) + S_{22}^{p-1}\mathrm{i}\,\mathbf{K}_\mathrm{I}(\Phi_{p-1}^+ - \Phi_{p-1}^-). \end{aligned} \tag{19}$$

From these equations it follows that $\Phi_{p-1}^- = \gamma_{p-1}\Phi_{p-1}^+$ where

$$\gamma_{p-1} = (\alpha_{p-1} + \beta_{p-1})^{-1}(\alpha_{p-1} - \beta_{p-1}) \qquad \alpha_{p-1} = S_{22}^{p-1}\mathrm{i}\,\mathbf{K}_\mathrm{I} + \mathbf{K}_\mathrm{I}\mathbf{R}_p S_{12}^{p-1}\mathbf{K}_\mathrm{I}$$

$$\beta_{p-1} = S_{21}^{p-1} + \mathrm{i}\,\mathbf{K}_\mathrm{I}\mathbf{R}_p S_{11}^{p-1} \qquad \mathbf{R}_p = (1-\gamma_p)(1+\gamma_p)^{-1}.$$

Hence by starting at the slice adjacent to the optical interface, and progressing slice by slice towards the vacuum, successively applying boundary conditions, we can evaluate the exit wavefunction for back-scattering, $\Phi_0^- = \mathbf{B}_0$.

The procedure outlined above now resembles the method recommended by Ichimiya [8] for the calculation of RHEED intensities more closely than the procedures in [5].

6. Computed intensities using the revised method

Figure 5 shows the results from a 13-beam calculation, for a thickness of 18 000 Å using one slice per Ångström (18 000 slices). The other parameters of the calculation are atom velocity: 600 m s^{-1}; field, 49 000 V m^{-1} and detuning: 2 GHz. These latter are the parameters used by Opat and Hajnal [1].

The main results are the sudden drop in the $n = 0$ intensity at around $\theta_{inc} = 7$ mrad and the rise in the $n = +1$ beam at that angle; and the further drop in the $n = 0$ beam at around $\theta_{inc} = 11$ mrad with the rise in the $n = +3$ beam. The +1 and +3 beams then reach 8% and 7% of incident beam value respectively. Of these the +1 beam has real propagation for all angles $0 \rightarrow 25$ mrad, while the +3 beam has a finite amplitude only in the range 11 mrad $\rightarrow$ 25 mrad. This latter result is consistent with the fact that the distance (from the interface) of 18 000 Å is sufficient for evanescent propagation (with $K_{yn}^2 < 0$), detected for this beam in the calculation at low angles, to be extinguished. The third most prominent diffraction order, for $n = +2$, which peaks at $\theta_{inc} = 16$ mrad is not plotted because its maximum value is a tenth that of the odd-order peaks.

Internal consistency of the calculation can be tested with respect to number of beams included and slice thickness, and the calculation can be considered optimized when either increasing the number of beams or the number of slices used to represent the same potential does not significantly change the results. Calculations were run separately with 11 and 13 beams for the above case; these two results for the central six beams are shown in table 2, as 'a' and 'b', for eight different incident angles. The differences between these two calculations are small for all beams which are above 1% (of the normalized incident beam) in intensity and insignificant for all beams above 10%, these differences being 10% and 1% (i.e. 1% and 0.1% of the incident beam in absolute terms) respectively. The one noticeable difference appearing in the table, in the entries for +2 beam for 16 mrad, arises from a very small shift in the angular position of the steep rise for that beam between the 11- and 13-beam calculations.

Such differences are an indication that 13 beams is still a conservative number for the precise location of such turning points. However, the conclusion reached here is that 13 beams are totally adequate for present experimental predictions. In a further test, further division of the 18 000 Å field by halving the slice thickness and using 36 000 slices produced no perceptible difference in the results, as is seen from the last two entries in table 2. This shows that the subdivision to 1 Å slices used here is sufficient to give convergence to the correct solution, and in fact is over-fine.

We conclude therefore that the peaks recorded in figure 5 are physically significant. These results show a pleasing degree of agreement with those obtained previously by a completely different approach [1], although these earlier results predicted higher $n = +2$ and +3 peaks and a lower +1 value. The characteristic feature which the two sets of curves have in common, that of the initial plateau for the $n = 0$ beam which terminates in a sudden drop, corresponds to a critical angle in wave optics, or a classical turning point in the equivalent particle model. The two calculations differ also in the location of this turning point (the present calculation giving 7 mrad compared with 10 mrad in [1]).

On the other hand, recent investigation by Deutschmann, Ertmer and Wallis [9] found that very little coupling to the diffraction orders occurred for similar conditions. However, their calculation was restricted to 2×2 matrices arranged in block-diagonal form within the $n \times n$ matrix. Many effects considered in our calculation such as evanescent atomic propagation and n-beam interactions were therefore omitted.

Finally, a calculation was made for smaller detuning, 1 GHz, and the results are shown

Table 2. Upper panel: intensities computed for diffraction orders for the two calculations of 11 and 13 beams (a and b) for the field depth 18 000 Å using 1 Å slices. The value of the incidence angle θ_{inc} is shown in the extreme left-hand column. Lower panel: intensities computed for diffraction orders for the two calculations for (c) 1 Å slices and (d) 0.5 Å slices, both for the field depth 18 000 Å and using 13 beams, calculated for $\theta_{inc} = 1$ mrad.

		Beam No					
θ_{inc} (mrad)		+3	+2	+1	0	−1	−2
1	a	0.140×10^{-16}	0.253×10^{-11}	0.788×10^{-5}	$0.100 \times 10^{+1}$	0.161×10^{-7}	0.202×10^{-6}
	b	0.790×10^{-17}	0.387×10^{-11}	0.122×10^{-4}	$0.100 \times 10^{+1}$	0.731×10^{-6}	0.182×10^{-6}
4	a	0.865×10^{-16}	0.726×10^{-11}	0.183×10^{-4}	$0.100 \times 10^{+1}$	0.120×10^{-5}	0.356×10^{-6}
	b	0.168×10^{-16}	0.532×10^{-11}	0.115×10^{-4}	$0.100 \times 10^{+1}$	0.270×10^{-6}	0.150×10^{-6}
7	a	0.335×10^{-13}	0.146×10^{-7}	0.577×10^{-1}	0.141	0.339×10^{-2}	0.333×10^{-2}
	b	0.319×10^{-13}	0.135×10^{-7}	0.537×10^{-1}	0.140	0.325×10^{-2}	0.267×10^{-2}
10	a	0.353×10^{-12}	0.321×10^{-7}	0.866×10^{-1}	0.463×10^{-1}	0.562×10^{-2}	0.302×10^{-2}
	b	0.329×10^{-12}	0.299×10^{-7}	0.808×10^{-1}	0.483×10^{-1}	0.551×10^{-2}	0.216×10^{-2}
13	a	0.115×10^{-1}	0.117×10^{-7}	0.242×10^{-1}	0.1248×10^{-1}	0.193×10^{-2}	0.105×10^{-3}
	b	0.395×10^{-1}	0.263×10^{-6}	0.214×10^{-1}	0.185×10^{-1}	0.165×10^{-2}	0.723×10^{-5}
16	a	0.327×10^{-1}	0.223×10^{-6}	0.114×10^{-1}	0.128×10^{-1}	0.353×10^{-3}	0.930×10^{-4}
	b	0.643×10^{-1}	0.203×10^{-1}	0.175×10^{-1}	0.104×10^{-1}	0.375×10^{-3}	0.117×10^{-3}
19	a	0.200×10^{-1}	0.898×10^{-2}	0.134×10^{-1}	0.239×10^{-2}	0.473×10^{-3}	0.130×10^{-4}
	b	0.287×10^{-1}	0.118×10^{-2}	0.139×10^{-1}	0.219×10^{-2}	0.390×10^{-3}	0.258×10^{-4}
22	a	0.813×10^{-2}	0.162×10^{-2}	0.769×10^{-2}	0.147×10^{-2}	0.325×10^{-3}	0.871×10^{-5}
	b	0.103×10^{-1}	0.684×10^{-5}	0.832×10^{-2}	0.124×10^{-2}	0.284×10^{-3}	0.183×10^{-4}
Beams							
11	c	0.164×10^{-16}	0.410×10^{-11}	0.763×10^{-5}	$0.100 \times 10^{+1}$	0.665×10^{-7}	0.203×10^{-6}
13	d	0.163×10^{-16}	0.399×10^{-11}	0.735×10^{-5}	$0.100 \times 10^{+1}$	0.666×10^{-7}	0.204×10^{-6}

in figure 6. This calculation shows a substantial increase in contribution to the $n = +1$ peak plus a longer tail to the $n = 0$ peak relative to the case with a detuning of 2 GHz.

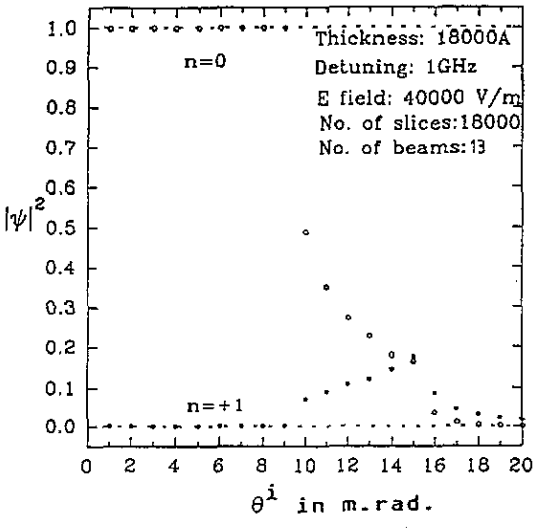

Figure 6. A similar plot to that in figure 5, only for a detuning of 1 GHz and a slightly reduced field strength of $E = 40000$ V cm^{-1}.

Acknowledgments

The authors gratefully acknowledge assistance received from Professor Robert March in the form of many helpful discussions, and to Dr Lloyd Hollenberg for checking the final manuscript. This project has been partly funded by Australian Research Council Small Grant No SG6923353.

References

[1] Hajnal J and Opat G 1989 *Opt. Commun.* **71** 119
[2] Hajnal J, Baldwin K G H, Fisk P T H, Bachor H-A and Opat G I 1989 *Opt. Commun.* **73** 331
[3] Goodman P and Moodie A F 1974 *Acta Crystallogr.* A **30** 280
[4] Lynch D F and Moodie A F 1972 *Surf. Sci.* **32** 422
[5] Lynch D F and Smith A E 1983 *Phys. Status Solidi* b **119** 355
[6] Cowley J M 1975 *Diffraction Physics* (Amsterdam: North-Holland) pp 203–4
[7] Collela R 1972 *Acta Crystallogr.* A **28** 11
[8] Ichimiya A 1983 *Japan. J. Appl. Phys.* **22** 176
[9] Deutschmann R, Ertmer W and Wallis H 1993 *Phys. Rev.* A **47** 42